Atmos. Chem. Phys. Discuss., 11, 15875–15920, 2011
www.atmos-chem-phys-discuss.net/11/15875/2011/
doi:10.5194/acpd-11-15875-2011

Atmospheric Chemistry and Physics Discussions

Measurements of aerosol charging states in Helsinki, Finland

S. Gagné[1], J. Leppä[2], T. Petäjä[1], M. J. McGrath[1], M. Vana[1,3], V.-M. Kerminen[2], L. Laakso[1,2,4], and M. Kulmala[1]

[1]Department of Physics, University of Helsinki, P.O. Box 64, 00014 Helsinki, Finland
[2]Finnish Meteorological Institute, Climate Change, P.O. Box 503, 00101 Helsinki, Finland
[3]Institute of Physics, University of Tartu, Ülikooli 18, 50090 Tartu, Estonia
[4]School of Physical and Chemical Sciences, North-West University, Private Bag x6001, Potchefstroom 2520, South Africa

Received: 10 February 2011 – Accepted: 17 May 2011 – Published: 26 May 2011

Correspondence to: S. Gagné (stephanie.gagne@helsinki.fi)

Published by Copernicus Publications on behalf of the European Geosciences Union.

Abstract

The charging state of aerosol populations was measured with an Ion-DMPS in Helsinki, Finland between December 2008 and February 2010. Based on the charging states, we calculated the ion-induced nucleation fraction to be around 0.8 % ± 0.9 %. We review the role of ion-induced nucleation and propose different explanations for a low ion-induced nucleation participation in urban areas. We present a new method to retrieve the average charging state for an event, and a given size. We also use a new theoretical framework that allows for different concentrations of small cluster ions for different polarities (polarity asymmetry). We extrapolate the ion-induced fraction using polarity symmetry and asymmetry. Finally, a method to calculate the growth rates from the variation of the charging state as a function of the particle diameter using polarity symmetry and asymmetry is presented and used on a selection of new particle formation events.

1 Introduction

The amount of particulate matter suspended in the air (aerosol) and its size distribution influence the Earth's climate and precipitation patterns (e.g. Twomey, 1991; Lohmann and Feichter, 2005; Myhre et al., 2009; Stevens and Feingold, 2009;). These particles can be emitted into the atmosphere directly (primary aerosols) or nucleate and grow in the atmosphere (secondary aerosols). The latter is commonly called new particle formation (NPF) and growth. Model simulations show that nucleation is a dominant source of particle number concentration in the atmosphere, and a significant contributor of cloud condensation nuclei (CCN, Spracklen et al., 2008; Merikanto et al., 2009; Pierce and Adams, 2009). New particle formation has been observed in a wide range of environments, and takes place frequently (e.g. Kulmala et al., 2004 and references therein). The frequency and the mechanisms involved in new particle formation depend on the type of environment where it takes place. For example, the phenomenon

ACPD
11, 15875–15920, 2011

has been observed to take place on almost every sunny day in the African Savannah (Laakso et al., 2008) while it is observed on about every third day in the Finnish boreal forest (Dal Maso et al., 2005) but almost never in the Amazon rain forest (Ahlm et al., 2010).

The mechanisms responsible for new particle formation and their relative contribution also varies from one place to another (Manninen et al., 2010) and from one day to another (Laakso et al., 2007a; Gagné et al., 2008 and 2010) and even during nucleation (Laakso et al., 2007b). There are many proposed nucleation mechanisms and their contributions are not well known. However, two general categories of mechanisms can be distinguished: neutral mechanisms and ion-induced mechanisms. Neutral mechanisms include all mechanisms that do not involve an electric charge. Ion-induced mechanisms are those that involve one or more electric charges in the formation process. The presence of electric charges can enhance the condensation of vapours onto the seed particle, at least in certain atmospheric conditions (Lovejoy et al., 2004; Curtius et al., 2006). Due to the large number of instruments capable of measuring air ions (Hirsikko et al., 2011) and those capable of measuring total particle size distribution, these two classes of mechanisms are relatively easy to distinguish and thus calculating the relative contribution of ion-induced nucleation to the new particle formation process is possible.

Several authors have studied the role of ion-induced nucleation in atmospheric new particle formation, both through modeling and measurements. Model simulations by Yu (2006, 2010) and Yu et al. (2008) and chamber experiment results Svensmark et al. (2007) indicate that ion-mediated nucleation may be an important global source of aerosols. The latter authors show a correlation between the production of aerosol particles, and thus CCN, by ion-induced nucleation and the 11-year solar cycle, which modulates the ionization rate of the atmosphere by galactic cosmic rays. However, both model and field measurements did not see any such correlation (Kazil et al., 2006; Kulmala et al., 2010). Several authors have found that negative and positive ions (charged particles) behaved in a different manner. At different rural sites (SMEAR

ACPD
11, 15875–15920, 2011

II station in Hyytiälä, Gagné et al., 2008 and 2010 and Tahkuse station in Estonia Hõrrak et al., 1998) days with negative overcharging are more frequent than days with positive overcharging (Vana et al., 2006; Laakso et al., 2007a; Gagné et al., 2008). This tendency is characteristic for measurement sites where ion-induced nucleation is sometimes important under favourable conditions.

In urban evironments, Iida et al. (2006) performed measurements near Boulder, Colorado and showed that the average contribution of ion-induced nucleation is about 0.5 % for both polarities, indicating that ion-induced nucleation is a relatively unimportant contributor to new particle formation. Furthermore, Iida et al. (2008) characterized the new particle formation events observed at Tecamac, Mexico, and found that the nucleated particles are initially almost all electrically neutral. Manninen et al. (2010) presented the ion-induced fraction for 12 different European sites using Neutral clusters and Air Ion Spectrometers (NAIS). NAISs and the Ion-DMPS yield comparable results Kerminen et al. (2010) and Gagné et al. (2010). The contribution of ion-induced nucleation to total particle formation at 2 nm was typically in the range of 1 to 30 %. The ion-induced contribution appeared to be smallest in more polluted continental sites. On the other hand, measurements in a clean marine coastal environment also show the general dominance of neutral nucleation pathways in new particle formation events (Ehn et al., 2010b).

In this study, we use Ion-DMPS (Ion-Differential Mobility Particle Sizer) measurements (Laakso et al., 2007a) performed at the SMEAR III station (Järvi et al., 2009), in Helsinki, Finland to estimate the contribution of ion-induced nucleation and neutral nucleation to new particle formation. Investigations of the ion-induced fraction in urban areas are rare. To our knowledge, this is only the third such report, after that of Iida et al. (2006 and 2008). We used the charging state (also called charging ratio) to retrieve the ion-induced fraction. The charging state is the ratio of the observed charged fraction to the steady-state charged fraction. We compare two analysis methods to calculate the charging ratio for each diameter. We describe the behaviour of the charging state without using the assumption that the number of cluster ions is the same for

ACPD
11, 15875–15920, 2011

both polarities, which was always assumed in previous studies. This set of equations is described in detail in Leppä et al. (2011). We use the method developed by Kerminen et al. (2007), with and without assuming the polarity symmetry, to extrapolate the charging state at 2 nm and subsequently calculate the contribution of ion-induced nucleation. We analysed our data set with each charging state analysis method in combination with each set of equations regarding the polarity symmetry assumption for a total of four methods. The growth rates in the size range 3–7 nm, 3–11 nm and 7–20 nm and the formation rates at 2 nm were calculated from DMPS measurements and are presented in this work. Finally, we use the variation of the charging ratio as a function of time to retrieve the growth rates, through a method adapted from Iida et al. (2008) by Leppä et al. (2011), also with and without the polarity symmetry assumption.

2 Instrumentation and methods

2.1 SMEAR III station

The site is considered a mildly polluted urban area. The Helsinki metropolitan area consists of 4 cities (Helsinki, Espoo, Vantaa and Kauniainen) accounting for a population of about one million inhabitants. The SMEAR III station (Station for Measuring Ecosystem-Atmosphere Relationships Järvi et al., 2009), situated in Helsinki, has been in operation since August 2004, after which more instruments have gradually been added. The station is situated in Kumpula, 5 km north-east of the Helsinki city center. Kumpula is situated close to a residential area, a small botanical garden and a park, as well as heavy traffic roads. According to Järvi et al. (2009), ultrafine particles are most influenced by the nearby traffic emissions. The Ion-DMPS was sampling from an inlet at the fourth floor of Kumpula's Physicum building, 40 m a.s.l. and about 20 m above the ground and at about 150 m north of the SMEAR III station. All the other instruments used in this study were situated either in a ground-level cottage or on the roof of the Physicum building (5 floors in total).

ACPD
11, 15875–15920, 2011

2.2 Ion-DMPS

The Ion-DMPS (Laakso et al., 2007a, and also Mäkelä et al., 2003; Iida et al., 2006) is an instrument based on a Differential Mobility Particle Sizer (DMPS, Aalto et al., 2001) with the addition of a few modifications that allow it to work in four different modes: (1) ambient negatively charged particles, (2) neutralized negatively charged particles, (3) ambient positively charged particles and (4) neutralized positively charged particles. A DMPS gives the size distribution of particles in time. First, the particles are charged to a known distribution through a neutralizer, then the particles are size segregated by a Differential Mobility Analyzer (DMA, Winklmayr et al., 1991) and, finally, counted with a particle counter (CPC, TSI 3025, Stolzenburg and McMurry, 1991). In the Ion-DMPS set-up, the neutralizer can be switched on or off, making it possible to measure in ambient and in neutralized mode with the same diffusional losses. Moreover, the voltage in the DMA can be negative or positive, so that particles of both polarities can be detected. By combining these two modifications, the Ion-DMPS measures the size distribution in the 4 modes enumerated above.

The Ion-DMPS was originally operating in a boreal forest environment at SMEAR II (Hari and Kulmala, 2005), Finland from April 2005 to November 2008 (results available in Laakso et al., 2007a; Gagné et al., 2008 and 2010). It was then moved to Helsinki to be used in the laboratory (Physicum) and was measuring outdoor air when it was not otherwise in use. The dataset analysed in this manuscript expands from 8 December 2008 until 24 February 2010. The Ion-DMPS was measuring outdoor air on roughly 60 % of the days during that period.

Due to higher particle concentrations at the urban SMEAR III station (Helsinki) compared to the background SMEAR II station (Hyytiälä), the Ion-DMPS was counting particles between 1.0 and 11.5 nm on 11 channels. The measurements of sub-3 nm particles are less reliable, because of the CPC's limitations and, on most days, no data points were available below this size. Due to these additional channels and adjustments in integration times, the 4-mode cycle lasted about 27 min.

ACPD
11, 15875–15920, 2011

All days on which the Ion-DMPS was measuring were classified into 3 categories: events, non-events, and undefined days, based on the classification described in Gagné et al. (2008). Event days were the days for which the Ion-DMPS detected appearance of new particles at small sizes, and their growth to the upper diameter range of the instrument. Non-event days were the days for which no such appearance or growth was seen. Days for which the data displayed either appearance of particles at small sizes but no growth or other unusual dynamical features were classified as undefined. Days on which only partial data was available, or on which the Ion-DMPS was not measuring, were not classified. Event days took place on 15 % of the classified days, 15 % were undefined and 70 % were non-event days.

Thirty-nine event days were found and further classified into undercharged, overcharged and steady-state days, using the method described in Laakso et al. (2007a) and Gagné et al. (2008, 2010). An overcharged particle population is defined as a population that has a higher fraction of charged particles than the steady-state charged fraction; oppositely, an undercharged particle population has a lower fraction of charged particles than the steady-state charged fraction. When the fraction is very close to the steady-state charged fraction, it is called steady-state. Due to the steady-state charged fraction being very small, and implying little ion-induced nucleation, steady-state events are grouped with undercharged events, as was done and explained in Gagné et al. (2010). For each event day, each polarity was classified by comparing the ambient and neutralized distributions. We also used data from a DMPS (Aalto et al., 2001) placed at the SMEAR III station and measuring in the 3–1000 nm size range, to estimate the growth rates and formation rates on those 39 days.

2.3 Analytical methods

2.3.1 Charging ratio retrieval: time averaging and slopes

There are several methods to calculate an average charging ratio for a given event. In this paper, we present two different methods: one that has been previously used and

ACPD
11, 15875–15920, 2011

one that had not been used until now for analysing Ion-DMPS data. The first method, described in more detail in Gagné et al. (2008), consists in calculating the charging ratio as a function of time, and averaging it over the time when new particle formation takes place (see Fig. 1). The second, new method was inspired from a method used to analyse Neutral cluster and Air Ion Spectrometer (NAIS) data, and described in Vana et al. (2006). The new method, adapted for Ion-DMPS data, is similar to the first method in that only one average value over the time span of the NPF event is obtained for each diameter. We first plot the concentration of ions in the ambient mode against the corresponding concentration of ions in the steady-state mode for the selected diameter and period. Then, a least-mean square fit is made through the points, forcing the fit through the origin. The slope is then the average charging ratio for the given diameter (see Fig. 2). The charging ratio as a function of the diameter is required to calculate the ion-induced fraction i.e. the fraction of new particles generated via ion-induced nucleation.

Each method has its own way of calculating uncertainties. The uncertainty of the diameter is common to both of them, and depends e.g. on flow fluctuations in the DMA as well as the DMA's transfer function. The uncertainty on the charging ratio, however, is calculated in different manners depending on the method. In the time averaged method, the uncertainty in the charging state depends on the integration time and the concentration of the CPC readings. In the slope method, the uncertainty is the sum of the uncertainty on the measurement point and the uncertainty attributable to the scatter around the linear fit.

2.3.2 Extrapolation of the charging state: polarity symmetry

In this paper, we use two different theoretical frameworks: one that assumes that the number concentration of small ions below 2 nm is the same for negative and positive ions ($N_C = N_C^- = N_C^+$ and $f^+ = f^-$), which we call polarity symmetry, and another described in Sect. 2.3.3 that does not make this assumption. The latter framework works with a different number concentration for negative and positive small ions ($N_C^- \neq N_C^+$),

ACPD
11, 15875–15920, 2011

which we call polarity asymmetry.

In the case where we assume polarity symmetry, the charging state S is the ratio of the ambient charged fraction to the neutralized charged fraction. Kerminen et al. (2007) developed an equation to describe the behaviour of the charging state S as a function of the diameter d_p:

$$S(d_p) = 1 - \frac{1}{K d_p} + \frac{(S_0 - 1)K d_0 + 1}{K d_p} e^{-K(d_p - d_0)} \quad (1)$$

where

$$K = \frac{\alpha N_C^{\pm}}{GR} \quad (2)$$

and S_0 and d_0 are the charging state and diameter of newly formed particles, respectively, $N_C^{\pm}$ is the number concentration of ion clusters, GR is the particle growth rate and α ($\sim 1.6 \times 10^{-6}\,cm^3 s^{-1}$) is the ion-ion recombination coefficient. Kerminen et al. (2007) make a number of assumptions that are all verified to be reasonable in the Helsinki atmospheric conditions (at least as much as they were for Hyytiälä conditions), with exception of the assumption that the concentration of ion clusters is the same for both polarities.

We therefore fitted Eq. (1) to the measured charging ratios with S_0 and K as free parameters. S_0 was limited to the maximum charging state possible (100 % of 2 nm particles charged) and −10 for a minimum. K was limited between 0.1 and 5 nm^{-1}. S_0 was allowed to go below zero, even though the value is non-physical, in order to allow more freedom in fitting the curve. The value of K becomes unrealistic below 0.1 nm^{-1} and the fit is no longer valid for very large values of K, hence an upper limit of 5 nm^{-1} example of the fitting was set for the fittings. However, all values above 2 were discarded in the quality check because at high values of K, the particle population does not bear memory of its previous charging state. The fitting method consisted of generating normally distributed points inside each measured point's uncertainty box (as

ACPD
11, 15875–15920, 2011

showed in Kerminen et al., 2007, Figs. 9, 10) and fit Eq. (1) through these points. Two thousand fits were made for each event day and polarity, the median S_0 value and its corresponding K value were taken as the representative values, along with the median absolute deviation (MAD) as an error estimate. An example of the fitting method is shown in Fig. 3.

The uncertainty of the charging ratio was slightly underestimated in the work of Kerminen et al. (2007) and Gagné et al. (2008), especially at larger diameters due to an error in the computer code. The mistake is corrected in this manuscript. The underestimation does not influence the conclusions of the above mentioned papers because the randomly generated points are normally distributed around the measured point. Hence, a small vertical extension of the boxes does not drastically change the distribution of points around the measured points. Moreover, two thousands fits were made per day and polarity, and only the median fit was kept so that the most extreme points do not have much influence on the average value. However, since a bigger uncertainty gives more freedom to the fittings, the values given for the median average deviation (MAD) may have been slightly underestimated for some days.

2.3.3 Extrapolation of the charging state: taking the polarity asymmetry into account

The equations used in this section are developed and explained in detail in Leppä et al. (2011). In this work, we apply this new theoretical framework to the Ion-DMPS measurements in Helsinki. If we reject the polarity symmetry assumption and instead use the framework of polarity asymmetry, i.e. when $N_C^- \neq N_C^+$ and $f^- \neq f^+$, the steady-state charged fraction is no longer estimated as $f_{eq} = \beta_0/\alpha$ (Kerminen et al., 2007). The ambient charged fraction will then approach the new equilibrium charged fraction, $f_{asy}^{\pm}$:

$$f_{asy}^{\pm} = \frac{\beta_0^{\pm} N_C^{\pm}}{\alpha N_C^{\mp}} = \frac{N_C^{\pm}}{N_C^{\mp}} f_{eq}^{\pm} \quad (3)$$

ACPD
11, 15875–15920, 2011

The charging state in the polarity symmetry assumption, S, is defined as the ratio of the ambient charged fraction and the charged fraction in bipolar charge equilibrium. We measure S with the Ion-DMPS, but we use an equivalent asymmetrical charging state, S_{asy}, such that:

$$S^{\pm}_{asy}(d_p) = 1 - \frac{1}{k^{\pm} d_p} + \frac{(S^{\pm}_{asy,0} - 1)k^{\pm} d_0 + 1}{k^{\pm} d_p} e^{-k^{\pm}(d_p - d_0)} \quad (4)$$

where

$$k^{\pm} = \frac{\alpha N_C^{\mp}}{GR} \quad (5)$$

In Eq. (4), the asymmetric charging state is defined as the ratio of the ambient charged fraction to the asymmetric charged fraction, $S^{\pm}_{asy} = f^{\pm}/f^{\pm}_{asy}$. $S^{\pm}_{asy}$ and S both tend to 1 when the diameter (d_p) increases in their respective equations (Eqs. 1 and 4). However, only the charging state S can be measured. Hence, when using the polarity asymmetry, we need to calculate $S^{\pm}_{asy}$ from $S^{\pm}$. We know $S^{\pm}_{asy} = f^{\pm}/f^{\pm}_{asy} = f^{\pm}/f_{eq} \cdot N_C^{\mp}/N_C^{\pm} = S^{\pm} \cdot N_C^{\mp}/N_C^{\pm}$. We can then use Eq. (4) to extrapolate the charging state at 2 nm. In this work, we used more than one year average of ion cluster concentration measured with a Balance Scanning Mobility Analyzer (BSMA) (Tammet, 2006). The average values we used were $N_C^{-} = 436$ and $N_C^{+} = 563\,cm^{-3}$, meaning that the concentration of positively charged clusters was slightly bigger than the concentration of negatively charged clusters.

2.3.4 Four methods to retrieve the ion-induced nucleation fraction

We presented two methods to retrieve the measured charged ratios for different diameters in Sect. 2.3.1 and two methods to extrapolate the charging state in Sects. 2.3.2 and 2.3.3 (using the polarity symmetry and asymmetry, respectively). We combined each of those methods to form four different methods. In order to insure the clarity of

ACPD
11, 15875–15920, 2011

the text, we renamed the four methods T0, TP, L0 and LP, according to the combination of methods used (Table 1). T represents the time average of the charging ratio, L represents charging ratios determined by slopes of linear fits through the concentrations in the ambient and neutralized modes, and 0 and P represent the symmetry assumption and the asymmetry inclusion for small ion concentrations, respectively. We consider LP to be the most advanced and reliable method of the four evaluated here.

2.3.5 Retrieving the growth rate from the charging state

Iida et al. (2008) developed a method to calculate the growth rate of a NPF event from the evolution of the charged fraction as a function of the diameter (GR_f). This method was developed because the growth rates in Mexico City were very high, and calculating them based on traditional methods (based on the particle size distribution, GR_{PSD}, Dal Maso et al., 2005) was difficult. The instruments they used (an Inclined Grid Mobility Analyzer, IGMA, and a specially modified DMPS) are similar but not identical to the Ion-DMPS. The method was applied on NPF events taking place in Mexico City (with higher growth rates) and in Boulder, Colorado (with lower growth rates) and agreed very well with GR_{PSD}.

The growth rates in Helsinki are generally small (below 5 nm h^{-1}) and can be calculated with traditional methods when the NPF event is dynamically well behaved. The modified method applied in this work rejects the polarity symmetry assumption. In cases where we have polarity symmetry, we have

$$GR_f = \frac{df}{dd_p}^{-1} N_C(\beta_o - \alpha f) \quad (6)$$

When we include the polarity asymmetry, we have

$$GR_f^{\pm} = \frac{df^{\pm}}{dd_p}^{-1} (\beta_o N_C^{\pm} - \alpha f^{\pm} N_C^{\mp}) \quad (7)$$

ACPD
11, 15875–15920, 2011

In the derivation of Eq. (7) all the particles are assumed to grow at the same rate, regardless of their size or charge (Leppä et al., 2011). Thus Eq. (7) should give the same growth rate for both polarities.

We applied this new method to NPF events in Helsinki, and compared the GR_f to GR_{PSD}. Only one value of df/dd_p was used for each day and polarity when determining GR using Eq. (7). The value of df/dd_p was determined as the slope of a first order polynomial (or straight line) fit to the values of charged fraction as a function of diameter. The GR was then estimated minimizing the least square difference between the measured charged fractions and charged fractions calculated using Eq. (7) with different values of GR. This procedure was then repeated 2000 times with values of f and corresponding dp taken randomly from around the measured values.

3 Results and discussion

3.1 General characteristics of the data set

Each day of the measurement period was examined in search of new particle formation events. The classification of the days into the event, non-event, undefined and event, non-event, undefined and no measurements category. is shown in Fig. 4, as a function of the month of the year. Unfortunately, there were no measurements made with the Ion-DMPS during the summer. However, based on DMPS measurements, only one NPF event took place during that time. Hussein et al. (2008) reported on several years of DMPS measurements in Helsinki and observed that the event frequency was higher in spring and autumn. Most of the events presented in this analysis are springtime events.

After finding 15 % of the days to be event days (39 events), we then further classified the events in overcharged and undercharged classes. For the negative polarity, we found two overcharged days and 35 undercharged days (including steady-state days), and it was impossible to make a decision for two days. For the positive polarity, we

ACPD
11, 15875–15920, 2011

found nine overcharged days, 28 undercharged days and two days were not classifiable. This may be an indication that the chemical or dynamical processes taking place in Helsinki are different from those observed at the SMEAR II rural station.

The formation and growth rates for each event were calculated using the method described by Kulmala et al. (2007) on DMPS data. The growth rates in the range 3–7 nm, 3–11 nm and 7–20 nm and new particle formation rates for 3 to 4 nm sized particles are presented in Table A1 (appendix) and summarized in Table 2. The growth rates in the literature are often divided into the 3–7 and 7–20 nm size ranges. In this paper, the growth rates in the 3–11 nm size range are of interest because this is also the Ion-DMPS size range, from which the growth rates have been calculated (see Sect. 3.3).

These 39 event days were selected based on Ion-DMPS data, however, the formation and growth rates were calculated based on DMPS data. It is thus very important to point out that most of the days in the list were not dynamically well-behaved event days. The classification of NPF events was also done based on DMPS data using the method described by Dal Maso et al. (2005). Class I (a and b) are days for which the formation and growth rates can be determined with a good confidence level while class II events are days for which it was not possible to determine those values at all, or the result may be questionable. Non-event days are the days where no NPF event took place. Finally, days were classified as undefined if it was not clear whether to classify them as event or non-event days. The DMPS classification of the 39 days presented in this work yielded only two type Ia events (21 March 2009 and 3 April 2009) and three type Ib events (19 March, 30 April and 14 October 2009). There were also seven type II events, three non-events and 22 undefined events, with the two remaining days not yet being classified. It must therefore be kept in mind that most of the values presented in Table 2 are only indicative. The growth rates in the 3–7 nm size range varied between 1.3 and 7.5 $\mathrm{nm\,h^{-1}}$ with a mean of 3.3 $\mathrm{nm\,h^{-1}}$. In the 3–11 and 7–20 nm size range, the growth rate varied between 1.5 and 6.9 $\mathrm{nm\,h^{-1}}$ with a mean of 3.2 $\mathrm{nm\,h^{-1}}$, and 1.1 and 17.7 $\mathrm{nm\,h^{-1}}$ with a mean of 4.3 $\mathrm{nm\,h^{-1}}$, respectively. Based on previous literature, growth rates are smaller for smaller particles and increase with increasing particle size

ACPD
11, 15875–15920, 2011

(Hirsikko et al., 2005; Riipinen et al., 2011). The total particle formation rates in the 3–4 nm size range varied between 0.1 and 3.8 $cm^{-3} s^{-1}$ with a mean of 0.8 $cm^{-3} s^{-1}$.

In the dataset presented here, one notices some differences between the rural (Hyytiälä) and urban (Helsinki) sites. In particular, most of the event days at the rural site are overcharged, while those in the urban area are undercharged. Also, one notices that the positive ions seem to be more involved in event days in Helsinki than in Hyytiälä. These observations raise two questions, which have not been conclusively answered in the literature, and which cannot be answered without further extensive observations and experiments.

The first question is, why does ion-induced nucleation appear to be less important in urban areas? One obvious response is that the concentration of ions is lower in urban areas than in rural environments. Ion production in the troposphere mostly happens through one of three mechanisms: cosmic rays, ground radiation (external radiation), and radon decay (this latter one is only important over continental landmasses, Laakso et al., 2004 and sources therein). No previous studies have pointed out a consistent difference between ion production rates in urban and rural environments, and therefore one cannot suppose that the production rates are different. However, small cluster ion concentrations have been noted to drop as air pollution increases. This is because the ions are effectively scavenged by larger aerosol clusters, which are present in polluted air (Jayaratne et al., 2008). This corresponding drop in small ion concentrations logically leads to a decrease in the importance of ion-induced nucleation. Another possible reason is that total nucleation rates are higher in urban environments, and if the charged nucleation rates are not scaled, then the fraction of ion-induced fraction decreases. This is consistent with Winkler et al. (2008) who show that negatively charged, followed by positively charged seeds activate with smaller vapour saturation ratios than neutral particles. Hence in urban environments when the condensing vapour concentrations are high, there is enough vapour for neutral nucleation to occur, making the fraction of ion-induced nucleation smaller. This is consistent with observations by Vana et al. (2006) and Gagné et al. (2010).

ACPD
11, 15875–15920, 2011

The second question is perhaps a little less straightforward to answer. Namely, why does the positive polarity seem to favor nucleation in Helsinki, while there are more overcharged days with negative polarity in Hyytiälä? A simple response to this question is that the positive ion concentration is higher in urban areas than in rural areas, an assertion that carries a little weight in the literature. One study performed in India in both a rural and urban site showed a preference for positive ions over negative ions (sometimes by a factor of two), which was attributed to negative ions being more likely to be absorbed by larger aerosols (Pawar et al., 2010). This ratio peaked in the early afternoon, which was attributed to the accumulation of human activity during the morning. Emphasis was placed on the fact that the rural site was undergoing extensive human agricultural activity. Ion concentration measurements in Hyytiälä revealed a small negative polarity preference (Manninen et al., 2009b), which can be attributed to the more pristine nature of the surrounding forest. By this same logic, the positive ion concentration in Helsinki should be somewhat higher than the negative ions, given the more polluted urban environment.

Most ion production sources in urban areas are bi-polar; that is, they produce positive and negative ions in approximately equal amounts (Ling et al., 2010). Two exceptions, according to the same authors, are power lines and substations, with power lines producing significantly more positive ions, and substations producing significantly more negative ions. These effects have been observed for hundreds of meters downwind of the high voltage power line (Matthews et al., 2008; Fews et al., 2002; Jayaratne et al., 2008). While there are no high voltage power lines near the Helsinki measuring station, there is a high-powered Doppler radar set on the same building. The radar itself, however, should not leak any ionizing radiation if it is working normally. The combination of surrounding positive ion sources and the higher scavenging effect of polluted air both would naturally lead to more overcharged event days for positive ions, assuming that the polarity of the ion does not have an effect on the ability of the ion to participate in ion-induced nucleation.

ACPD
11, 15875–15920, 2011

This last assumption is not trivial. It is not known if the sign of the ion affects the nucleation rate. At first glance, one would not think so. However, bases (in particular ammonia and amines) are widely considered to be critical in ion-induced nucleation (by stabilizing small sulphuric acid complexes, Kurtén et al., 2008). Recent results have shown that negative ionic aerosols are composed of acids, while positive ions are composed of bases (Ehn et al., 2010a). If bases are important, and if bases only appear in small positive charged ions, then it follows that positively charged clusters should be more able to spark nucleation than negatively charged clusters. For example, one can imagine a positively charged ion being solvated by water molecules. These water molecules should be oriented so that the negatively charged oxygen is pointed towards the ion, while the hydrogens are dangling away from it. These dangling hydrogens would make a base much more likely to attach to the cluster, possibly resulting in a partial proton transfer, such as a low-barrier hydrogen bond. This would explain the results presented in this paper for Helsinki, but unfortunately does not shine light on why the situation is reversed in the rural site of Hyytiälä.

3.2 Ion-induced fraction

Each of the days that were classified as event days were analysed with each of the four methods. Tables B1, B2, B3 and B4 in the appendix show the results for methods T0, TP, L0 and LP, respectively. The results of all four methods are summarized in Table 3. All four methods yielded similar results: a low participation of ion-induced nucleation to new particle formation events measured in Helsinki.

Tables B1–B4 present the date in the first column followed by the median extrapolated charging state at 2 nm (S_0), its associated K value, the MAD of the 2000 fits and the quality of the fit for each polarity. Finally, the last two columns show the fraction of ion-induced nucleation taking part in the NPF event, and its MAD. The quality assessment of the fits as well as the rejection of data points was the same for all four methods. The quality of the fit is 1 if the median fit passes through every data-box, 2 if the fit passes though most boxes or if there exists no data below 5 nm, and 3 if the

ACPD
11, 15875–15920, 2011

fit ignores the tendencies seen from the data points or if there is not enough data at smaller sizes. When the fit quality was 3, the fitting parameters were all removed (indicated by "–"). Fits with a median charging ratio smaller than zero (non-physical result) are set to zero and their MAD removed. Fits with K values larger than 2 were also removed because large values of K indicate that the information about the charging state is lost before we can measure it, around 3 nm (see Kerminen et al. (2007) and Gagné et al. (2008) for more explanations about the memory phenomena associated with the K parameter).

We compare the methods, based on Table 3. All the values estimating uncertainty were smaller for the L methods (L0 and LP) than for the T methods (MADs = 0.8 % and 0.9 % rather than 1.6 % and 1.8 %, for L and T methods, respectively). This suggests that the slope method was more stable than the time averaged method. Moreover, fewer fits were rejected when the charging ratio was retrieved using the linear regression method (slope method) than when it was determined by the median charging ratio of the NPF period (time averaged method). The addition of the polarity asymmetry (P methods) did not have a big effect on the ion-induced fractions, nor on their MAD. The polarity asymmetry becomes more important when using the charging ratio to retrieve growth rates, as will be discussed in Sect. 3.3. The P methods gave slightly higher median values than their 0 counterparts. The same method applied to a sample of overcharged events from Hyytiälä showed no such tendency. As the difference between the methods is well within the MAD and the standard deviation of the sample, the polarity asymmetry method does not seem to be an important phenomena in these particular conditions.

The T0 method was used by Gagné et al. (2008) in Hyytiälä. They observed a median contribution of ion-induced nucleation of 6.4 % (MAD = 2.0 %). The median contribution in Helsinki, using the same method, was 0.8 % (MAD = 1.6 %, mean = 1.5 % and standard deviation = 2.0 %). With the most up to date method (LP), the median ion-induced nucleation fraction was 0.8 % (MAD = 0.9 %, mean = 1.0 % and standard deviation = 0.7 %).

ACPD
11, 15875–15920, 2011

Figure 5 shows the extrapolated ion-induced nucleation fraction at 2 nm, according to the LP method, as a function of the day of year. No clear seasonal tendency was observed in the variation of the ion-induced fraction. The majority of event days saw a contribution of ion-induced nucleation below 1 %, with a maximum of 2.9 %. All events but two had contributions below 2 %.

3.3 Growth rates

We calculated the growth rates for every day using a method based on the particle size distribution (GR_{PSD}, Hirsikko et al., 2005) as well as the method based on the charging state (GR_f) described in Sect. 2.3.5. It proved difficult to apply both methods because the NPF events in Helsinki were not dynamically well-behaved. The GR_{PSD} based on DMPS measurements are presented in Table 4.

The growth rates were generally small (below 5 nm h^{-1}). Iida et al. (2008) and Kerminen et al. (2007) both showed, with slightly different methods, that when the growth rate is small, the charged particles have enough time to recombine and thus loose their initial charge information before they can reach measurable sizes. In the work of Iida et al. (2008), the smallest GR_{PSD} was 3.9 nm h^{-1}, while in this work it varied between 1.3 and 7.5 nm h^{-1} with a median of 3.3 nm h^{-1}. The numbers stated above include all 39 days used in this study. However, as mentioned earlier, only class I events can deliver reliable growth rates. Hence, if we limit ourselves to well-behaved events, the values of GR_{PSD} should be reliable within a factor of two (Manninen et al., 2009a) and all the growth rates are smaller than 3 nm h^{-1}. In Fig. 6, we present only the points that belong to Class I events, according to the classification of Dal Maso et al. (2005). The uncertainty on GR_{PSD} is shown by horizontal bars and those on GR_f by vertical bars.

For both the asymmetric and the symmetric method, the GR_f are overestimated if we consider the GR_{PSD} to be reference values. In the symmetric case, the growth rates are closer to GR_{PSD} for the positive polarity and further away for negative polarity. One should remember that the number of positive small ions was larger than that of negative

ACPD
11, 15875–15920, 2011

small ions. When the asymmetry of small ion concentration is introduced, the growth rates of each polarity move closer to each other. The growth rates become closer to the expected value for negative particles while the growth rates for positive particles move further away from GR_{PSD}. The growth rates determined using Eq. (6) seem to be constantly higher than those determined from particle size distributions. There are at least two possible explanations for this: the concentrations of charged clusters are significantly different than the average values used here, or the df/dd_p is too small. The first cannot be verified because the concentrations were not measured, but it seems unlikely that their concentrations would have varied constantly in a way to yield higher growth rates when using Eqs. (6) and (7). It is possible that the charged fraction could not be measured adequately with the Ion-DMPS, due to low size and time resolutions.

4 Conclusions

In this work, we presented an analysis of 39 new particle formation events based on the Ion-DMPS classification scheme. We used a new method to calculate the charging state at each diameter that had never before been used on Ion-DMPS data. We also applied, for the first time, the theoretical background to calculate the charging state without assuming that the concentration of clusters is the same for negatively and positively charged particles. To our knowledge, it is the first time that the polarity asymmetry was taken into account in estimating the charging state and the ion-induced fraction from measurements. We made an analysis of four methods using a combination of the following: (a) using either a time average of the charging ratio or the slope of the least mean square fit of the concentrations in ambient and neutralized modes; and (b) using the polarity symmetry or the polarity asymmetry. We found that the method using the slope of the concentrations is superior to the time averaged method, reducing the MAD by almost a factor of two. We also observed that the inclusion of the polarity asymmetry does not make much difference when it comes to determining the ion-induced fraction, at least in the conditions presented here.

ACPD
11, 15875–15920, 2011

We used a method to estimate growth rates from the evolution of the charged fraction (GR_f) that we compared with the traditional particle size distribution-based method GR_{PSD}. GR_f is a method modified from that described and used by Iida et al. (2008). The modified method can also be used assuming the polarity symmetry or asymmetry. We found that taking into account the polarity asymmetry made the growth rates of negative and positive polarity closer to each other, improving the results. However, the GR_f values seemed systematically overestimated, probably due to too small variations in the charged fraction as a function of the diameter or instrumental errors.

Finally, we found that the ion-induced fraction in Helsinki was about 0.8 % on average. This is consistent with the ion-induced fractions observed in other urban environments. Possible reasons for the difference between urban and rural environments could be that the concentration of small ions in urban environments are smaller than in remote areas. The scavenging of small ions is more important in polluted environments, and therefore small ions are less likely to participate in nucleation. The apparent importance of positively charged ions over negatively charged ions could be explained by negative ions being scavenged more easily or by the presence of bases (contributing to positive ion nucleation) in greater concentrations than acids (contributing to negative ion nucleation).

Acknowledgements. This research was supported by the Academy of Finland Center of Excellence program (project number 1118615), and the European Commission 6th Framework program project EUCAARI, contract no 036833-2 (EUCAARI). Bjarke Molgaard is acknowledged for providing the DMPS event classification. Petri Keronen and Pasi P. Aalto are acknowledged for maintaining the SMEAR III station and providing the DMPS data.

References

Aalto, P. P., Hämeri, K., Becker, E., Weber, R., Salm, J., Mäkelä, J. M., Hoell, C., O'Dowd, C. D., Karlsson, H., Hansson, H.-C., Väkevä, M., Koponen, I. K., Buzorius, G., and Kulmala, M.: Physical characterization of aerosol particles during nucleation events, Tellus, 53B, 344–358, 2001. 15880, 15881

ACPD
11, 15875–15920, 2011

Ahlm, L., Nilsson, E. D., Krejci, R., Mårtensson, E. M., Vogt, M., and Artaxo, P.: A comparison of dry and wet season aerosol number fluxes over the Amazon rain forest, Atmos. Chem. Phys., 10, 3063–3079, doi:10.5194/acp-10-3063-2010, 2010. 15877

Curtius, J., Lovejoy, E. R., and Froyd, K. D.: Atmospheric ion-induced aerosol nucleation, Space Sci. Rev., 125, 159–167, 2006. 15877

Dal Maso, M., Kulmala, M., Riipinen, I., Wagner, R., Hussein, T., Aalto, P. P., and Lehtinen, K. E. J.: Formation and Growth of Fresh Atmospheric Aerosols: Eight Years of Aerosol Size Distribution Data from SMEAR II, Hyytiälä, Finland, Boreal Environmental Research, 10, 323–336, 2005. 15877, 15886, 15888, 15893

Ehn, M., Junninen, H., Petäjä, T., Kurtén, T., Kerminen, V.-M., Schobesberger, S., Manninen, H. E., Ortega, I. K., Vehkemäki, H., Kulmala, M., and Worsnop, D. R.: Composition and temporal behavior of ambient ions in the boreal forest, Atmos. Chem. Phys., 10, 8513–8530, doi:10.5194/acp-10-8513-2010, 2010. 15891

Ehn, M., Vuollekoski, H., Petäjä, T., Kerminen, V.-M., Vana, M., Aalto, P. P., de Leeuw, G., Ceburnis, D., Dupuy, R., ODowd, C. D., and Kulmala, M.: Growth rates during coastal and marine new particle formation in western Ireland, J. Geophys. Res., 115, D18 218, doi:10.1029/2010JD014292, 2010b. 15878

Fews, A. P., Wilding, R. J., Keitch, P. A., Holden, N. K., and Henshaw, D. L.: Modification of atmospheric DC fields by space charge from high-voltage power lines, Atmos. Res., 63, 271–289, 2002. 15890

Gagné, S., Laakso, L., Petäjä, T., Kerminen, V.-M., and Kulmala, M.: Analysis of one year of Ion-DMPS data from the SMEAR II station, Finland, Tellus, 60B, 318–329, 2008. 15877, 15878, 15880, 15881, 15882, 15884, 15892

Gagné, S., Nieminen, T., Kurtén, T., Manninen, H. E., Petäjä, T., Laakso, L., Kerminen, V.-M., Boy, M., and Kulmala, M.: Factors influencing the contribution of ion-induced nucleation in a boreal forest, Finland, Atmos. Chem. Phys., 10, 3743–3757, doi:10.5194/acp-10-3743-2010, 2010. 15877, 15878, 15880, 15881, 15889

Hõrrak, U., Salm, J., and Tammet, H.: Bursts of intermediate ions in atmospheric air, J. Geophys. Res., 103, D12, 13 909–13 915, 1998. 15878

Hari, P. and Kulmala, M.: Station for Measuring Ecosystem-Atmosphere Relations (SMEAR II), Boreal Env. Res., 10, 315–322, 2005. 15880

Hirsikko, A., Laakso, L., Hõrrak, U., Aalto, P. P., Kerminen, V.-M., and Kulmala, M.: Annual and size dependent variation of growth rates and ion concentrations in boreal forest, Boreal

ACPD
11, 15875–15920, 2011

Environment Research, 10, 357–369, 2005. 15889, 15893
Hirsikko, A., Nieminen, T., Gagn, S., Lehtipalo, K., Manninen, H. E., Ehn, M., Hõrrak, U., Kerminen, V.-M., Laakso, L., McMurry, P. H., Mirme, A., Mirme, S., Petäjä, T., Tammet, H., Vakkari, V., Vana, M., and Kulmala, M.: Atmospheric ions and nucleation: a review of observations, Atmos. Chem. Phys., 11, 767–798, doi:10.5194/acp-11-767-2011, 2011. 15877
Hussein, T., Martikainen, J., Junninen, H., Sogacheva, L., Wagner, R., Dal Maso, M., Riipinen, I., Aalto, P. P., and Kulmala, M.: Observation of regional new particle formation in the urban atmosphere, Tellus, 60B, 509–521, 2008. 15887
Iida, K., Stolzenburg, M. R., McMurry, P. H., Dunn, M. J., Smith, J. N., Eisele, F., and Keady, P.: Contribution of ion-induced nucleation to new particle formation: Methodology and its application to atmospheric observations in Boulder, Colorado, J. Geophys. Res., 111, d23201, doi:10.1029/2006JD007167, 2006. 15878, 15880
Iida, K., Stolzenburg, M. R., McMurry, P. H., and Smith, J. N.: Estimating nanoparticle growth rates from size-dependent charged fractions: Analysis of new particle formation events in Mexico City, J. Geophys. Res., 113, d05207, doi:10.1029/2007JD009260, 2008. 15878, 15879, 15886, 15893, 15895
Järvi, L., Hannuniemi, H., Hussein, T., Junninen, H., Aalto, P. P., Hillamo, R., Mäkelä, T., Keronen, P., Siivola, E., Vesala, T., and Kulmala, M.: The urban measurement station SMEAR III: Continuous monitoring of air pollution and surface-atmosphere interactions in Helsinki, Finland, Boreal Environment Research, 14 (suppl. A), 86–109, d05207, doi:10.1029/2007JD009260, 2009. 15878, 15879
Jayaratne, E. R., J-Fatokun, F. O., and Morawska, L.: Air ion concentrations under overhead high-voltage transmission lines, Atmos. Environ., 42, 1846–1856, 2008. 15889, 15890
Kazil, J., Lovejoy, E. R., Barth, M. C., and O'Brien, K.: Aerosol nucleation over oceans and the role of galactic cosmic rays, Atmos. Chem. Phys., 6, 4905–4924, doi:10.5194/acp-6-4905-2006, 2006. 15877
Kerminen, V.-M., Anttila, T., Petäjä, T., Laakso, L., Gagné, S., Lehtinen, K. E. J., and Kulmala, M.: Charging state of the atmospheric nucleation mode: Implications for separating neutral and ion-induced nucleation, J. Geophys. Res., 112, d21205, doi:10.1029/2007JD008649, 2007. 15879, 15883, 15884, 15892, 15893
Kerminen, V.-M., Petäjä, Manninen, H. E., Paasonen, P., Nieminen, T., Sipilä, M., Junninen, H., Ehn, M., Gagné, S., Laakso, L., Riipinen, I., Vehkamäki, H., Kurtén, T., Ortega, I., Dal Maso,

ACPD
11, 15875–15920, 2011

M., Brus, D., Hyvärinen, A., Lihavainen, H., Leppä, J., Lehtinen, K. E. J., Mirme, A., Mirme, S., Hõrrak, U., Berndt, T., Stratmann, F., Birmili, W., Wiedensohler, A., Metzger, A., Dommen, J., Baltensperger, U., Kiendler-Scharr, A., Mentel, A., Wildt, J., Winkler, P., Wagner, P. E., Petzgold, A., Minikin, A., Plass-Dülmer, C., Pöschl, U., Laaksonen, A., and Kulmala, M.: Atmospheric nucleation: highlights of the EUCAARI project and future directions, Atmos. Chem. Phys., 10, 10829–10848, doi:10.5194/acp-10-10829-2010, 2010. 15878

Kulmala, M., Vehkamäki, H., Petäjä, T., Dal Maso, M., Lauri, A., Kerminen, V.-M., Birmili, W., and McMurry, P. H.: Formation and growth rates of ultrafine atmospheric particles: a review of observations, J. Aerosol Sci., 35, 143–176, 2004. 15876

Kulmala, M., Riipinen, I., Sipilä, M., Manninen, H. E., Petäjä, T., Junninen, H., Dal Maso, M., Mordas, G., Mirme, A., Vana, M., Hirsikko, A., Laakso, L., Harrison, R. M., Hanson, I., Leung, C., Lehtinen, K. E. J., and Kerminen, V.: Toward direct measurement of atmospheric nucleation, Science, 318, 89–92, 2007. 15888

Kulmala, M., Riipinen, I., Nieminen, T., Hulkkonen, M., Sogacheva, L., Manninen, H. E., Paasonen, P., Petäjä, T., Dal Maso, M., Aalto, P. P., Viljanen, A., Usoskin, I. Vainio, R., Mirme, S., Mirme, A., Minikin, A., Petzold, A., Hõrrak, U., Plass-Dülmer, C., Birmili, W., and Kerminen, V.-M.: Atmospheric data over a solar cycle: no connection between galactic cosmic rays and new particle formation, Atmos. Chem. Phys., 10, 1885–1898, doi:10.5194/acp-10-1885-2010, 2010. 15877

Kurtén, T., Loukonen, V., Vehkamäki, H., and Kulmala, M.: Amines are likely to enhance neutral and ion-induced sulfuric acid-water nucleation in the atmosphere more effectively than ammonia, Atmos. Chem. Phys., 8, 4095–4103, doi:10.5194/acp-8-4095-2008, 2008. 15891

Laakso, L., Petäjä, T., Lehtinen, K. E. J., Kulmala, M., Paatero, J., Hõrrak, U., Tammet, H., and Joutsensaari, J.: Ion production rate in a boreal forest based on ion, particle and radiation measurements, Atmos. Chem. Phys., 4, 1933–1943, doi:10.5194/acp-4-1933-2004, 2004. 15889

Laakso, L., Gagné, S., Petäjä, T., Hirsikko, A., Aalto, P. P., Kulmala, M., and Kerminen, V.-M.: Detecting charging state of ultra-fine particles: instrumental development and ambient measurements, Atmos. Chem. Phys., 7, 1333–1345, doi:10.5194/acp-7-1333-2007, 2007. 15877, 15878, 15880, 15881

Laakso, L., Grönholm, T., Kulmala, L., Haapanala, S., Hirsikko, A., Lovejoy, E. R., Kazil, J., Kurtén, T., Boy, M., Nilsson, E. D., Sogachev, A., Riipinen, I., Stratmann, F., and Kulmala, M.: Hot-air balloon as a platform for boundary layer profile measurements during particle

ACPD
11, 15875–15920, 2011

formation, Boreal Environment Research, 12, 279–294, 2007b. 15877
Laakso, L., Laakso, H., Aalto, P. P., Keronen, P., Petäjä, T., Nieminen, T., Pohja, T., Siivola, E., Kulmala, M., Kgabi, N., Molefe, M., Mabaso, D., Phalatse, D., Pienaar, K., and Kerminen, V.-M.: Basic characteristics of atmospheric particles, trace gases and meteorology in a relatively clean Southern African Savannah environment, Atmos. Chem. Phys., 8, 4823–4839, doi:10.5194/acp-8-4823-2008, 2008. 15877
Leppä, J., Gagné, S., Laakso, L., Kulmala, M., and Kerminen, V.-M.: Title to be announced, in preparation, 2011. 15879, 15884, 15887
Ling, X., Jayaratnea, R., and Morawska, L.: Air ion concentrations in various urban outdoor environments, Atmos. Environ., 44 (18), 2186–2193, 2010. 15890
Lohmann, U. and Feichter, J.: Global indirect aerosol effects: a review, Atmos. Chem. Phys., 5, 715–737, doi:10.5194/acp-5-715-2005, 2005. 15876
Lovejoy, E. R., Curtius, J., and Froyd, K. D.: Atmospheric ion-induced nucleation of sulfuric acid and water, J. Geophys. Res., 109, D08204, doi:10.1029/2003JD004460, 2004. 15877
Mäkelä, J. M., Salm, J., Smirnov, V. V., Koponen, I., Paatero, J., and Pronin, A. A.: Electrical charging state of fine and ultrafine particles in boreal forest air, J. Aerosol Sci., 32, S149–S150, 2003. 15880
Manninen, H. E., Nieminen, T., Riipinen, I., Yli-Juuti, T., Gagné, S., Asmi, E., Aalto, P. P., Petäjä, T., Kerminen, V.-M., and Kulmala, M.: Charged and total particle formation and growth rates during EUCAARI 2007 campaign in Hyytiälä, Atmos. Chem. Phys., 9, 4077–4089, doi:10.5194/acp-9-4077-2009, 2009. 15893
Manninen, H. E., Petäjä, T., Asmi, E., Riipinen, I., Nieminen, T., Mikkilä, J., Hõrrak, U., Mirme, A., Mirme, S. Laakso, L., , Kerminen, V.-M., and Kulmala, M.: Long-term field measurements of charged and neutral clusters using Neutral cluster and Air Ion Spectrometer (NAIS), Boreal Environmental Research, 14, 591–605, 2009b. 15890
Manninen, H. E., Nieminen, T., Asmi, E., Gagné, S., Häkkinen, S., Lehtipalo, K., Aalto, P., Vana, M., Mirme, A., Mirme, S., Hõrrak, U., Plass-Dülmer, C., Stange, G., Kiss, G., Hoffer, A., Törö, N., Moerman, M., Henzing, B., de Leeuw, G., Brinkenberg, M., Kouvarakis, G. N., Bougiatioti, A., Mihalopoulos, N., O'Dowd, C., Ceburnis, D., Arneth, A., Svenningsson, B., Swietlicki, E., Tarozzi, L., Decesari, S., Facchini, M. C., Birmili, W., Sonntag, A., Wiedensohler, A., Boulon, J., Sellegri, K., Laj, P., Gysel, M., Bukowiecki, N., Weingartner, E., Wehrle, G., Laaksonen, A., Hamed, A., Joutsensaari, J., Petj, T., Kerminen, V.-M., and Kulmala, M.: EUCAARI ion spectrometer measurements at 12 European sites - analysis of new particle formation

ACPD
11, 15875–15920, 2011

events, Atmos. Chem. Phys., 10, 7907–7927, doi:10.5194/acp-10-7907-2010, 2010. 15877, 15878
Matthews, J. C., Buckley, A. J., Keitch, P. A., Wright, M. D., and Henshaw, D. L.: Measurements of corona ion induced atmospheric electricity modification near to HV power lines, J. Phys. Conf. Ser., 142, 012044, doi:10.1088/1742-6596/142/1/012044 2008. 15890
Merikanto, J., Spracklen, D. V., Mann, G. W., Pickering, S. J., and Carslaw, K. S.: Impact of nucleation on global CCN, Atmos. Chem. Phys., 9, 8601–8616, doi:10.5194/acp-9-8601-2009, 2009. 15876
Myhre, G., Berglen, T. F., Johnsrud, M., Hoyle, C. R., Berntsen, T. K., Christopher, S. A., Fahey, D. W., Isaksen, I. S. A., Jones, T. A., Kahn, R. A., Loeb, N., Quinn, P., Remer, L., Schwarz, J. P., and Yttri, K. E.: Modelled radiative forcing of the direct aerosol effect with multi-observation evaluation, Atmos. Chem. Phys., 9, 1365–1392, doi:10.5194/acp-9-1365-2009, 2009. 15876
Pawar, S. D., Meena, G. S., and Jadhav, D. B.: Diurnal and Seasonal Air Ion Variability at Rural Station Ramanandnagar ($17^{o'}2N, 74^{\circ}E$), India, Aerosol Air Qual. Res., 10, 154–166, 2010. 15890
Pierce, J. R. and Adams, P. J.: Uncertainty in global CCN concentrations from uncertain aerosol nucleation and primary emission rates, Atmos. Chem. Phys., 9, 1339–1356, doi:10.5194/acp-9-1339-2009, 2009. 15876
Riipinen, I., Pierce, J. R., Yli-Juuti, T., Nieminen, T., Hkkinen, S., Ehn, M., Junninen, H., Lehtipalo, K., Petj, T., Slowik, J., Chang, R., Shantz, N. C., Abbatt, J., Leaitch, W. R., Kerminen, V.-M., Worsnop, D. R., Pandis, S. N., Donahue, N. M., and Kulmala, M.: Organic condensation: a vital link connecting aerosol formation to cloud condensation nuclei (CCN) concentrations, Atmos. Chem. Phys., 11, 3865–3878, doi:10.5194/acp-11-3865-2011, 2011. 15889
Spracklen, D. V., Carslaw, K. S., Kulmala, M., Kerminen, V.-M., Sihto, S.-L., Riipinen, I., Merikanto, J., Mann, G. W., Chipperfield, M. P., Wiedensohler, A., Birmili, W., and Lihavainen, H.: Contribution of particle formation to global cloud condensation nuclei concentrations, Geophys. Res. Lett., 35, L06, 808, 2008. 15876
Stevens, B. and Feingold, G.: Untangling aerosol effects on clouds and precipitation in a buffered system, Nature, 461, 607–613, 2009. 15876
Stolzenburg, M. R. and McMurry, P. H.: An ultrafine aerosol condensation nucleus counter, Aerosol Sci. Technol., 14, 48–65, 1991. 15880
Svensmark, H., Pedersen, J. O., Marsh, N. D., Enghoff, M. B., and Uggerhj, U. I.: Experimental

ACPD
11, 15875–15920, 2011

evidence for the role of ions in particle nucleation under atmospheric conditions, Proc. R. Soc. A, 463, 385–396, 2007. 15877

Tammet, H.: Continuous scanning of the mobility and size distribution of charged clusters and nanometer particles in atmospheric air and the Balanced Scanning Mobility Analyzer BSMA, Atmos. Res., 82, 523–535, 2006. 15885

Twomey, S.: Aerosols, clouds and radiation, Atmos. Environ., 25A, 2435–2442, 1991. 15876

Vana, M., Tamm, E., Hõrrak, U., Mirme, A., Tammet, H., Laakso, L., Aalto, P. P., and Kulmala, M.: Charging state of atmospheric nanoparticles during the nucleation burst events, Atmos. Res., 82, 536–546, 2006. 15878, 15882, 15889

Winkler, P. M., Steiner, G., Virtala, A., Vehkamäki, H., Noppel, M., Lehtinen, K. E. J., Reischl, G. P., Wagner, P. E., and Kulmala, M.: Heterogeneous Nucleation Experiments Bridging the Scale from Molecular Ion Clusters to Nanoparticles, Science, 319, 1374, doi:10.1126/science. 1149034, 2008. 15889

Winklmayr, W., Reischl, G. P., Lindner, A. O., and Berner, A.: A new electromobility spectrometer for the measurement of aerosol size distributions in the size range from 1 to 1000 nm, J. Aerosol Sci., 22, 289–296, 1991. 15880

Yu, F.: From molecular clusters to nanoparticles: second-generation ion-mediated nucleation model, Atmos. Chem. Phys., 6, 5193–5211, doi:10.5194/acp-6-5193-2006, 2006. 15877

Yu, F.: Ion-mediated nucleation in the atmosphere: Key controlling parameters, implications, and look-up table, J. Geophys. Res., 115, D03 206, doi:10.1029/2009JD012630, 2010. 15877

Yu, F., Wang, Z., Luo, G., and Turco, R.: Ion-mediated nucleation as an important global source of tropospheric aerosols, Atmos. Chem. Phys., 8, 2537–2554, doi:10.5194/acp-8-2537-2008, 2008. 15877

ACPD

11, 15875–15920, 2011

Table 1. Simplified names for each method based on the combination of the charging ratio averaging and the inclusion of the polarity asymmetry to the fits to Eq. (1). T represents the median charging ratio during the time of the NPF event and L represents the slope of a linear fit through the concentration of particles in the ambient mode as a function of the concentration of particles in the neutralized mode. The letters T and L are combined with either 0, representing the polarity symmetry assumption for the concentration of clusters in both polarities, or P, representing the use of the polarity asymmetry.

	Polarity symmetry	*P*olarity asymmetry
*T*ime average of the charging ratio	T0	TP
Slopes of the *L*inear fits	L0	LP

ACPD
11, 15875–15920, 2011

Table 2. Statistics on the growth and formation rates based on DMPS data (refer to Table 4 in the appendix for the full list of days). The statistical operation is in the first column (median, mean, standard deviation, minimum and maximum). The growth rates in the 3–7 nm size range (second column) is followed by the growth rates in the 3–11 and 7–20 nm size range. Finally, the total 3–4 nm particle formation rates are shown in the last column.

	GR_{3-7}	GR_{3-11}	GR_{7-20}	J_{tot3-4}
median	3.3	2.7	3.3	0.7
mean	3.3	3.2	4.3	0.8
std	1.5	1.5	4.1	0.8
min	1.3	1.5	1.1	0.1
max	7.5	6.9	17.7	3.8

ACPD
11, 15875–15920, 2011

Table 3. This table summarizes the ion-induced fraction (IIN) and its median absolute deviation (MAD) statistics for each method: T0, TP, L0 and LP. All values are taken from Tables B1 to B4 in Appendix B.

	T0		TP		L0		LP	
	IIN	MAD	IIN	MAD	IIN	MAD	IIN	MAD
median	0.8	1.6	1.2	1.8	0.7	0.8	0.8	0.9
mean	1.5	1.9	1.6	2.8	0.9	1.1	1.0	1.1
std	2.0	1.2	1.7	3.0	0.8	0.6	0.7	0.5
min	0.0	0.4	0.0	0.2	0.1	0.3	0.3	0.4
max	10.4	4.3	9.0	13.1	3.6	2.2	2.9	2.3
rejected	26 %	59 %	23 %	41 %	23 %	31 %	15 %	21 %

ACPD
11, 15875–15920, 2011

Appendix A

Event growth and formation rates derived from the DMPS

Table A1. Growth and formation rates based on DMPS data, for each day classified as an event day according to the Ion-DMPS classification scheme. The date is presented in the first column, followed by the day of year. The growth rates in the 3–7 nm size range is in the third column followed by the growth rates in the 3–11 and 7–20 nm size ranges. Finally, the 3–4 nm total new particle formation rates are shown in the last column. The table's statistics are presented at the end of the table.

Date	DoY	GR_{3-7}	GR_{3-11}	GR_{7-20}	J_{tot3-4}
1 Jan 2009	1	2.5	2.5	4.2	0.1
4 Jan 2009	4	–	–	–	0.2
16 Jan 2009	16	1.3	1.6	3.3	0.5
31 Jan 2009	31	3.4	1.7	2.9	0.8
9 Feb 2009	40	4.2	5.9	–	1.4
25 Feb 2009	56	3.7	2.1	1.2	0.7
19 Mar 2009	78	3.8	2.8	2.3	0.5
20 Mar 2009	79	–	–	–	1.1
21 Mar 2009	80	3.2	2.4	1.7	0.7
22 Mar 2009	81	1.3	2.3	1.3	0.7
23 Mar 2009	82	–	–	–	1.0
25 Mar 2009	84	–	–	–	0.5
26 Mar 2009	85	–	1.5	1.6	–
27 Mar 2009	86	–	–	–	0.5
1 Apr 2009	91	–	–	–	1.2
3 Apr 2009	93	7.5	2.2	2.7	2.7
8 Apr 2009	98	–	–	–	0.7
9 Apr 2009	99	1.8	4.6	3.5	0.4
18 Apr 2009	108	–	3.6	3.7	0.7
19 Apr 2009	109	4.0	4.1	8.1	0.9
30 Apr 2009	120	–	–	4.1	0.4

ACPD
11, 15875–15920, 2011

Table A1. Continued.

Date	DoY	GR_{3-7}	GR_{3-11}	GR_{7-20}	J_{tot3-4}
1 May 2009	121	–	–	2.6	0.6
2 May 2009	122	–	–	2.4	0.7
3 May 2009	123	1.6	2.7	4.0	0.2
7 May 2009	127	–	–	–	–
8 May 2009	128	–	–	–	2.5
12 May 2009	132	3.3	3.6	4.4	0.4
11 Sep 2009	254	3.1	6.18	15.1	0.5
12 Sep 2009	255	–	–	–	0.8
13 Sep 2009	256	3.9	6.9	17.7	0.2
6 Oct 2009	279	–	2.4	5.1	–
10 Oct 2009	283	3.1	3.0	1.1	0.7
11 Oct 2009	284	4.1	3.3	4.2	3.8
14 Oct 2009	287	–	2.1	1.4	0.4
23 Jan 2010	23	–	–	–	–
14 Feb 2010	45	–	–	–	0.1
15 Feb 2010	46	–	–	–	–
20 Feb 2010	51	–	4.15	–	0.9
24 Feb 2010	55	–	–	–	0.2
median		3.3	2.7	3.3	0.7
mean		3.3	3.2	4.3	0.8
std		1.5	1.5	4.1	0.8
min		1.3	1.5	1.1	0.1
max		7.5	6.9	17.7	3.8

ACPD
11, 15875–15920, 2011

Appendix B

Fit parameters for all analysed days and all methods

Table B1. Results for the median S_0 fit for each day for method T0: time average of the charging ratio, polarity symmetry.

Date	S_0^-	K^-	MAD S_0^-	Q	S_0^+	K^+	MAD S_0^+	Q	IIN (%)	MAD IIN
1 Jan 2009	0.88	0.11	0.58	2	0.88	0.12	0.57	2	1.39	0.91
4 Jan 2009	4.78	0.10	1.83	2	1.04	0.18	0.30	2	4.75	1.74
16 Jan 2009	0.83	0.31	2.55	1	0.15	0.10	0.58	2	0.80	2.55
31 Jan 2009	0.31	0.31	4.26	2	0.22	0.10	0.20	2	0.42	3.69
9 Feb 2009	1.66	0.15	0.42	1	0.89	0.10	0.76	2	2.05	0.92
25 Feb 2009	0.00	0.46	–	2	0.86	0.10	0.26	2	0.65	–
19 Mar 2009	0.00	0.69	–	2	0.47	0.10	0.85	2	0.35	–
20 Mar 2009	1.48	1.47	0.97	2	0.94	0.10	0.21	2	1.93	0.96
21 Mar 2009	0.00	0.53	–	1	0.88	0.11	0.58	2	0.66	–
22 Mar 2009	0.54	0.44	2.39	1	0.42	0.16	0.69	3	0.76	2.50
23 Mar 2009	0.00	0.41	–	2	0.00	0.10	–	2	0.00	–
25 Mar 2009	0.00	0.37	–	2	0.61	0.19	0.81	2	0.46	–
26 Mar 2009	0.00	0.54	–	2	–	–	–	3	–	–
27 Mar 2009	–	–	–	3	0.69	0.10	0.39	2	–	–
1 Apr 2009	0.78	0.15	1.23	2	0.03	0.15	0.51	2	0.67	1.40
3 Apr 2009	0.00	1.56	–	2	–	–	–	3	–	–
8 Apr 2009	0.47	0.46	1.34	2	0.73	0.17	0.69	2	0.94	1.63
9 Apr 2009	1.48	0.13	0.34	1	0.12	0.16	0.27	2	1.32	0.48
18 Apr 2009	0.00	0.71	–	2	0.75	0.17	0.10	2	0.56	–
19 Apr 2009	–	–	–	2	0.73	0.28	0.11	2	–	–
30 Apr 2009	0.94	0.62	0.10	1	1.26	0.10	0.45	2	1.73	0.42
1 May 2009	1.91	0.57	1.65	2	0.48	0.10	0.25	2	1.95	1.56
2 May 2009	0.00	0.80	–	2	1.01	0.10	0.67	1	0.76	–

ACPD
11, 15875–15920, 2011

Table B1. Continued.

Date	S_0^-	K^-	MAD S_0^-	Q	S_0^+	K^+	MAD S_0^+	Q	IIN (%)	MAD IIN
3 May 2009	0.00	0.85	–	2	3.70	0.16	0.67	2	2.78	–
7 May 2009	0.00	0.70	–	2	0.57	0.15	0.32	2	0.43	–
8 May 2009	0.00	0.32	–	2	0.62	0.23	0.28	2	0.47	–
12 May 2009	0.36	0.49	4.29	2	0.66	0.18	0.33	2	0.79	3.81
11 Sep 2009	0.00	0.73	–	1	1.48	0.10	0.69	1	1.11	–
12 Sep 2009	0.00	1.19	–	2	1.48	0.19	1.75	2	1.11	–
13 Sep 2009	1.69	0.33	4.66	2	1.22	0.15	0.56	2	2.32	4.29
6 Oct 2009	–	–	–	3	–	–	–	3	–	–
10 Oct 2009	–	–	–	3	–	–	–	3	–	–
11 Oct 2009	–	–	–	3	–	–	–	3	–	–
14 Oct 2009	0.00	0.46	–	2	–	–	–	3	–	–
23 Jan 2010	–	–	–	3	0.00	0.10	–	2	–	–
14 Feb 2010	–	–	–	3	0.32	0.10	2.26	2	–	–
15 Feb 2010	12.48	0.18	6.10	2	0.00	0.19	–	2	10.36	–
20 Feb 2010	1.30	0.27	1.74	2	0.26	0.10	0.46	2	1.27	1.79
24 Feb 2010	0.35	0.48	0.29	1	0.59	0.10	0.95	2	0.73	0.95
median	0.33	0.46	1.65		0.66	0.11	0.54		0.80	1.59
mean	1.01	0.53	2.04		0.73	0.14	0.58		1.50	1.85
std	2.31	0.36	1.78		0.67	0.05	0.45		1.95	1.20
min	0.00	0.10	0.10		0.00	0.10	0.10		0.00	0.42
max	12.48	1.56	6.10		3.70	0.28	2.26		10.36	4.29

ACPD
11, 15875–15920, 2011

Table B2. Results for the median S_0 fit for each day for method TP: time average of the charging ratio, polarity asymmetry.

Date	S^-_{0asy}	K^-_{asy}	MAD S^-_{0asy}	Q	S^+_{0asy}	K^+_{asy}	MAD S^+_{0asy}	Q	IIN (%)	MAD IIN
1 Jan 2009	1.23	0.10	0.81	2	3.08	0.10	3.29	2	3.77	3.71
4 Jan 2009	1.56	0.10	0.43	2	0.21	0.78	1.57	1	1.21	1.80
16 Jan 2009	0.30	0.36	0.82	2	0.75	0.10	1.66	2	0.92	2.13
31 Jan 2009	0.43	0.10	0.21	2	1.11	0.10	0.28	2	1.35	0.41
9 Feb 2009	1.30	0.10	1.01	1	2.88	0.10	12.90	2	3.62	13.14
25 Feb 2009	1.25	0.10	0.34	2	0.48	0.30	9.48	2	1.27	9.40
19 Mar 2009	0.41	0.97	1.34	2	0.83	0.33	0.54	2	1.07	1.38
20 Mar 2009	1.33	0.16	0.32	2	0.45	0.20	1.71	2	1.29	1.86
21 Mar 2009	1.24	0.17	0.74	1	0.33	0.44	1.25	2	1.12	1.69
22 Mar 2009	0.50	0.32	0.95	1	0.77	0.29	3.06	2	1.07	3.57
23 Mar 2009	0.00	0.22	–	1	0.28	0.41	1.92	2	0.27	–
25 Mar 2009	0.66	0.32	1.20	1	1.09	0.56	2.02	2	1.48	2.73
26 Mar 2009	0.47	0.24	1.45	2	1.03	0.66	0.95	2	1.30	1.85
27 Mar 2009	1.13	0.10	0.46	2	0.41	0.10	0.90	2	1.12	1.17
1 Apr 2009	0.00	0.38	–	1	0.00	0.28	–	2	0.00	–
3 Apr 2009	0.46	0.42	0.48	2	0.60	0.35	0.51	2	0.88	0.80
8 Apr 2009	0.90	0.20	0.91	2	1.00	0.16	0.25	2	1.55	0.83
9 Apr 2009	0.00	0.22	0.39	2	0.00	0.32	–	2	0.00	–
18 Apr 2009	0.96	0.38	0.14	2	0.71	1.08	0.09	2	1.30	0.18
19 Apr 2009	0.92	0.56	0.12	2	–	–	–	2	–	–
30 Apr 2009	1.79	0.42	0.54	2	1.19	0.16	1.12	2	2.30	1.43
1 May 2009	–	–	–	3	0.00	0.19	–	2	–	–
2 May 2009	1.34	0.10	1.01	2	0.00	0.29	–	2	0.86	–

ACPD
11, 15875–15920, 2011

Table B2. Continued.

Date	S^{-}_{0asy}	K^{-}_{asy}	MAD S^{-}_{0asy}	Q	S^{+}_{0asy}	K^{+}_{asy}	MAD S^{+}_{0asy}	Q	IIN (%)	MAD IIN
3 May 2009	7.93	0.37	3.90	2	0.00	0.31	–	2	5.10	–
7 May 2009	0.73	0.10	0.46	2	0.10	0.10	3.02	2	0.57	3.22
8 May 2009	1.02	0.10	0.33	2	0.63	0.10	2.80	2	1.27	2.92
12 May 2009	0.92	0.34	0.46	2	0.05	0.57	0.93	1	0.64	1.20
11 Sep 2009	2.07	0.35	1.03	1	0.00	0.33	–	1	1.33	–
12 Sep 2009	1.81	0.15	5.57	2	–	–	–	3	–	–
13 Sep 2009	1.81	0.17	0.70	1	8.12	0.42	5.79	2	9.03	6.06
6 Oct 2009	–	–	–	3	–	–	–	3	–	–
10 Oct 2009	–	–	–	3	–	–	–	3	–	–
11 Oct 2009	–	–	–	3	–	–	–	3	–	–
14 Oct 2009	1.32	0.10	4.64	2	–	–	–	3	–	–
23 Jan 2010	–	–	–	3	0.77	0.11	1.42	2	–	–
14 Feb 2010	–	–	–	3	11.48	0.26	7.38	2	–	–
15 Feb 2010	0.00	0.10	–	2	0.52	0.10	1.32	2	0.50	–
20 Feb 2010	0.37	0.12	0.63	2	0.33	0.16	0.21	2	0.56	0.61
24 Feb 2010	0.76	0.14	1.26	2	0.14	0.10	0.99	2	0.62	1.77
median	0.92	0.17	0.72		0.52	0.28	1.42		1.16	1.80
mean	1.12	0.24	1.09		1.19	0.30	2.49		1.58	2.78
std	1.35	0.18	1.30		2.37	0.23	3.04		1.78	3.04
min	0.00	0.10	0.12		0.00	0.10	0.09		0.00	0.18
max	7.93	0.97	5.57		11.48	1.08	12.90		9.03	13.14

ACPD
11, 15875–15920, 2011

Table B3. Results for the median S_0 fit for each day for method L0: slope of the linear fit passing through the concentration in the ambient mode as a function of concentration in the neutralized mode, polarity symmetry.

Date	S_0^-	K^-	MAD S_0^-	Q	S_0^+	K^+	MAD S_0^+	Q	IIN (%)	MAD IIN
1 Jan 2009	0.44	0.41	0.55	2	2.58	1.09	2.32	2	2.30	2.20
4 Jan 2009	0.13	0.17	0.54	1	–	–	–	2	–	–
16 Jan 2009	0.37	0.16	0.48	1	0.75	0.32	0.78	2	0.87	0.98
31 Jan 2009	0.01	0.10	0.50	1	0.13	0.26	0.46	1	0.11	0.76
9 Feb 2009	0.25	0.10	0.42	1	4.52	0.10	2.18	2	3.60	1.98
25 Feb 2009	0.49	0.23	0.40	2	0.65	1.33	1.78	2	0.89	1.67
19 Mar 2009	0.41	0.40	0.41	1	0.00	1.13	–	1	0.34	–
20 Mar 2009	0.57	0.10	0.39	1	0.32	0.65	0.39	1	0.71	0.62
21 Mar 2009	0.93	0.32	0.52	2	0.08	0.62	0.77	2	0.83	1.01
22 Mar 2009	0.65	0.45	0.48	2	–	–	–	3	–	–
23 Mar 2009	0.13	0.10	0.33	1	0.55	0.10	0.42	2	0.52	0.59
25 Mar 2009	0.21	0.13	0.38	1	0.48	0.66	0.51	1	0.53	0.70
26 Mar 2009	0.49	0.10	0.46	2	0.48	0.18	0.72	2	0.77	0.92
27 Mar 2009	0.44	0.10	0.42	2	0.75	0.10	0.73	1	0.93	0.90
1 Apr 2009	0.25	0.18	0.31	1	0.25	0.39	0.38	2	0.40	0.54
3 Apr 2009	0.39	0.10	0.37	1	0.11	0.47	0.41	1	0.41	0.61
8 Apr 2009	0.17	0.13	0.33	2	0.30	0.15	0.61	1	0.37	0.73
9 Apr 2009	0.54	0.15	0.52	2	0.11	0.25	0.47	2	0.53	0.78
18 Apr 2009	0.42	0.59	0.22	2	0.43	0.66	0.21	2	0.67	0.34
19 Apr 2009	–	–	–	3	–	–	–	3	–	–
30 Apr 2009	0.99	0.10	0.63	1	0.18	0.30	0.38	2	0.96	0.81
1 May 2009	0.33	0.10	0.38	1	0.12	0.14	0.39	1	0.36	0.61
2 May 2009	0.55	0.10	0.52	1	0.44	0.21	0.33	2	0.79	0.68
3 May 2009	–	–	–	2	1.91	0.20	1.81	2	–	–
7 May 2009	0.32	0.10	0.53	1	0.00	0.18	–	2	0.27	–
8 May 2009	0.16	0.13	0.38	1	0.28	0.18	0.52	1	0.34	0.71

ACPD
11, 15875–15920, 2011

Table B3. Continued.

Date	S_0^-	K^-	MAD S_0^-	Q	S_0^+	K^+	MAD S_0^+	Q	IIN (%)	MAD IIN
12 May 2009	0.59	0.10	0.53	1	2.07	0.45	1.60	2	2.04	1.64
11 Sep 2009	1.18	0.10	1.11	1	0.58	0.25	0.96	2	1.41	1.64
12 Sep 2009	0.40	0.27	0.65	1	0.51	0.39	0.64	1	0.71	1.02
13 Sep 2009	–	–	–	3	–	–	–	3	–	–
6 Oct 2009	–	–	–	3	–	–	–	3	–	–
10 Oct 2009	–	–	–	3	–	–	–	3	–	–
11 Oct 2009	0.79	0.10	1.25	2	0.84	0.29	1.20	2	1.29	1.94
14 Oct 2009	1.05	0.10	1.39	2	0.00	0.29	–	2	0.87	–
23 Jan 2010	0.00	0.10	–	1	–	–	–	3	–	–
14 Feb 2010	0.00	0.10	–	2	–	–	–	3	–	–
15 Feb 2010	0.14	0.10	0.77	1	0.50	0.13	1.22	2	0.49	1.55
20 Feb 2010	0.17	0.12	0.29	1	0.28	0.22	0.39	1	0.35	0.53
24 Feb 2010	2.77	0.10	1.77	2	0.51	0.10	0.95	1	2.68	2.18
median	0.41	0.10	0.48		0.44	0.26	0.63		0.71	0.81
mean	0.49	0.17	0.57		0.67	0.38	0.84		0.91	1.06
std	0.50	0.12	0.34		0.93	0.32	0.59		0.79	0.56
min	0.00	0.10	0.22		0.00	0.10	0.21		0.11	0.34
max	2.77	0.59	1.77		4.52	1.33	2.32		3.60	2.20

ACPD
11, 15875–15920, 2011

Table B4. Results for the median S_0 fit for each day for method LP: slope of the linear fit passing through the concentration in the ambient mode as a function of concentration in the neutralized mode, polarity asymmetry.

Date	S^-_{0asy}	K^-_{asy}	MAD S^-_{0asy}	Q	S^+_{0asy}	K^+_{asy}	MAD S^+_{0asy}	Q	IIN (%)	MAD IIN
1 Jan 2009	0.49	0.22	0.68	1	1.18	0.32	1.06	2	1.46	1.46
4 Jan 2009	0.02	0.23	0.51	1	1.20	0.31	1.11	2	1.18	1.40
16 Jan 2009	0.48	0.30	0.56	2	0.72	0.15	0.61	2	1.01	0.95
31 Jan 2009	0.06	0.13	0.50	1	0.22	0.14	0.48	1	0.25	0.79
9 Feb 2009	0.28	0.35	0.45	1	2.76	0.75	2.01	1	2.85	2.24
25 Feb 2009	0.60	0.22	0.50	2	0.55	0.43	0.60	2	0.92	0.90
19 Mar 2009	0.48	0.25	0.44	1	0.00	0.23	–	2	0.31	–
20 Mar 2009	0.73	0.26	0.43	2	0.37	0.23	0.34	2	0.83	0.61
21 Mar 2009	1.12	0.21	0.66	1	0.18	0.65	0.55	1	0.89	0.96
22 Mar 2009	0.85	0.10	0.61	2	0.20	0.39	0.45	2	0.74	0.83
23 Mar 2009	0.14	0.14	0.36	1	0.49	0.11	0.40	1	0.56	0.62
25 Mar 2009	0.22	0.17	0.38	1	0.48	0.44	0.46	1	0.61	0.69
26 Mar 2009	0.64	0.12	0.54	2	0.46	0.15	0.63	2	0.86	0.96
27 Mar 2009	0.60	0.36	0.56	2	0.51	0.10	0.60	1	0.88	0.94
1 Apr 2009	0.27	0.16	0.31	1	0.33	0.27	0.36	2	0.49	0.55
3 Apr 2009	0.45	0.16	0.36	2	0.18	0.23	0.43	1	0.46	0.65
8 Apr 2009	0.18	0.38	0.34	2	0.32	0.15	0.59	1	0.43	0.79
9 Apr 2009	0.69	0.14	0.63	2	0.20	0.18	0.43	1	0.64	0.82
18 Apr 2009	–	–	–	3	0.38	0.49	0.20	2	–	–
19 Apr 2009	0.60	0.10	0.29	2	0.45	0.74	0.21	2	0.82	0.39
30 Apr 2009	1.47	0.11	0.86	1	0.32	0.34	0.35	2	1.25	0.89
1 May 2009	0.40	0.12	0.41	1	0.23	0.14	0.41	1	0.48	0.66
2 May 2009	0.63	0.14	0.57	1	0.47	0.20	0.38	1	0.86	0.73
3 May 2009	0.68	0.17	1.42	2	1.38	0.66	1.09	2	1.77	1.97
7 May 2009	0.37	0.10	0.58	1	0.04	0.16	0.47	2	0.28	0.83
8 May 2009	0.19	0.10	0.39	1	0.26	0.12	0.49	1	0.37	0.73

ACPD
11, 15875–15920, 2011

Table B4. Continued.

Date	S^{-}_{0asy}	K^{-}_{asy}	MAD S^{-}_{0asy}	Q	S^{+}_{0asy}	K^{+}_{asy}	MAD S^{+}_{0asy}	Q	IIN (%)	MAD IIN
12 May 2009	0.82	1.07	0.67	2	1.46	0.18	1.03	2	1.94	1.43
11 Sep 2009	1.57	0.11	1.39	1	0.48	0.16	0.76	2	1.47	1.63
12 Sep 2009	0.48	0.18	0.74	1	0.46	0.21	0.56	1	0.75	1.02
13 Sep 2009	1.11	0.11	1.17	2	–	–	–	3	–	–
6 Oct 2009	–	–	–	3	–	–	–	3	–	–
10 Oct 2009	–	–	–	3	–	–	–	3	–	–
11 Oct 2009	0.99	0.19	1.48	2	0.75	0.19	1.02	2	1.36	1.94
14 Oct 2009	1.15	0.10	1.69	2	0.00	0.14	–	2	0.74	–
23 Jan 2010	0.02	0.10	0.97	1	–	–	–	3	–	–
14 Feb 2010	0.00	0.10	–	2	–	–	–	3	–	–
15 Feb 2010	0.16	0.10	0.81	2	0.44	0.10	1.09	2	0.53	1.58
20 Feb 2010	0.23	0.15	0.31	1	0.26	0.15	0.37	1	0.40	0.56
24 Feb 2010	3.96	0.14	2.32	2	0.30	0.10	0.81	1	2.84	2.28
median	0.49	0.15	0.56		0.41	0.20	0.52		0.82	0.89
mean	0.64	0.20	0.71		0.53	0.27	0.64		0.95	1.06
std	0.69	0.17	0.46		0.53	0.19	0.37		0.65	0.51
min	0.00	0.10	0.29		0.00	0.10	0.20		0.25	0.39
max	3.96	1.07	2.32		2.76	0.75	2.01		2.85	2.28

ACPD
11, 15875–15920, 2011

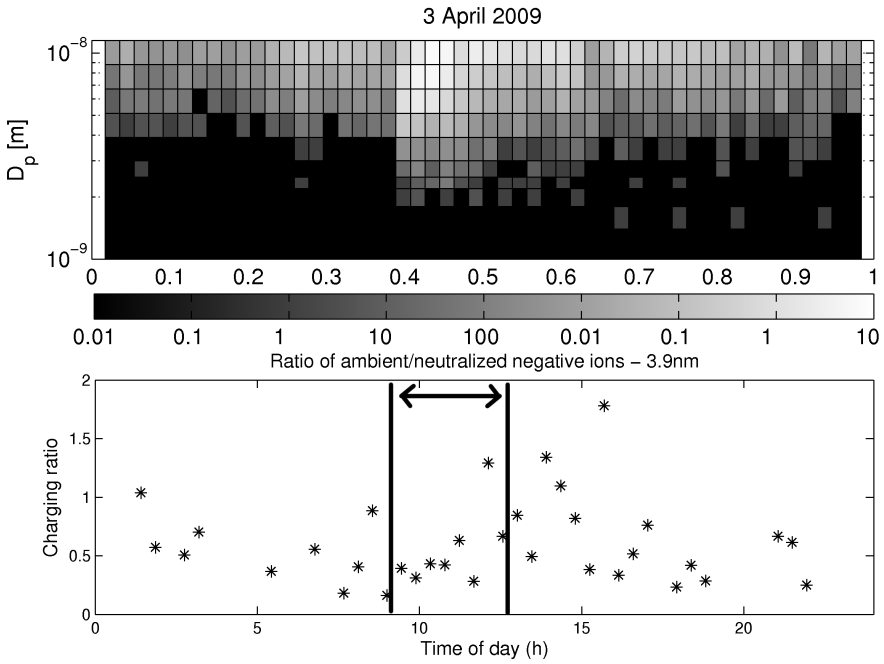

Fig. 1. Example of the determination of the average charging ratio at 3.9 nm for 3 April 2009, negative polarity for the time averaged method. The charging ratio is plotted as a function of time. The data-analyst chooses the time span of new particle formation for the relevant diameter, indicated here by the vertical bars in the lower panel. The median charging ratio is kept as the average value.

ACPD
11, 15875–15920, 2011

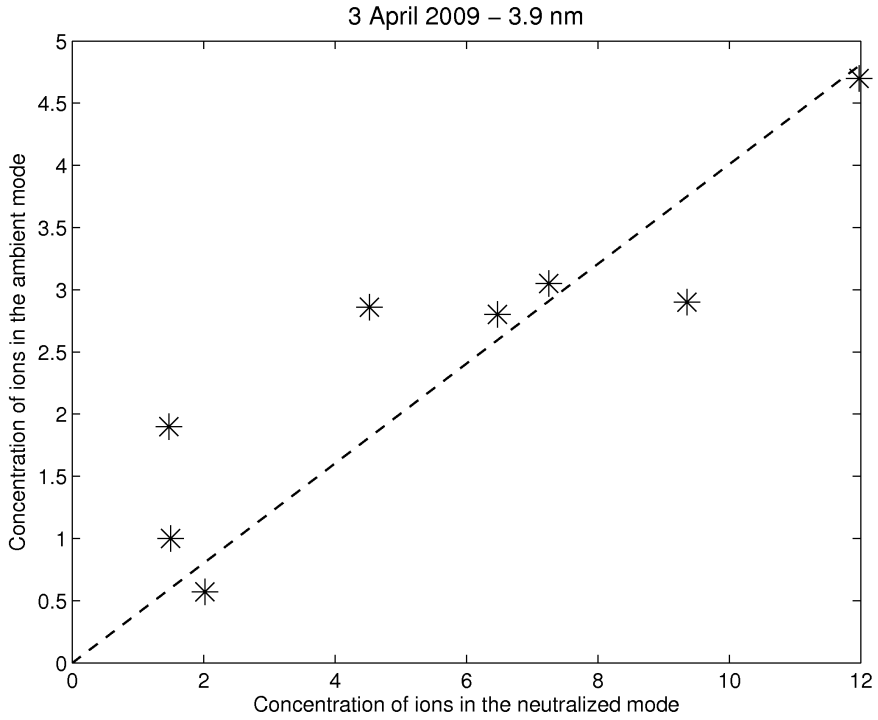

Fig. 2. Example of the determination of the average charging ratio at 3.9 nm for 3 April 2009, negative polarity for the slope method. The time span was the same as the one selected in Fig. 1. The concentration of charged particles in ambient mode is plotted as a function of the concentration in neutralized mode, so that the slope of the fit (force to intercept the origin) is the average charging ratio at the given particle size.

ACPD
11, 15875–15920, 2011

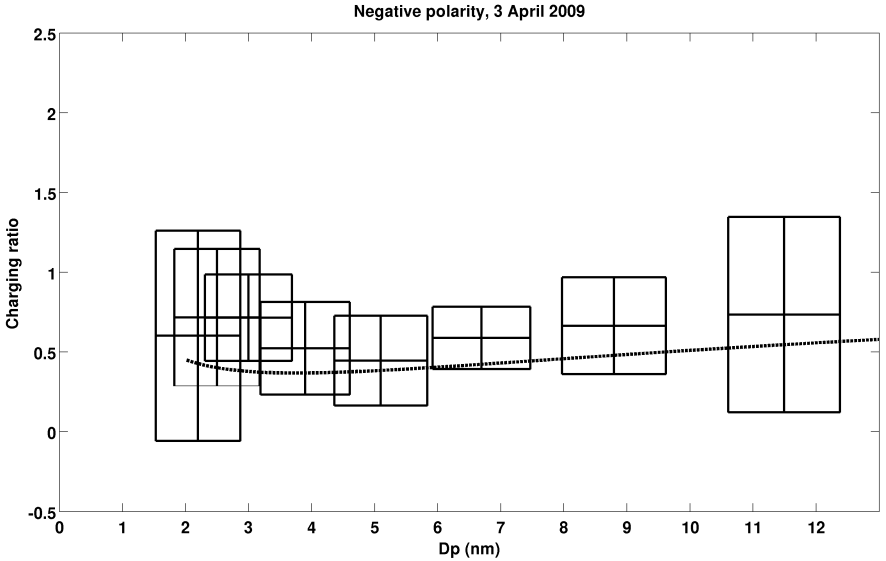

Fig. 3. Example of a fit to Eq. (1). Example of a fit for 3 April 2009, negative polarity. The middle of the boxes represent the measured points and the boxes around them, the uncertainty. The dashed line represents the fit (out of the 2000 generated fits) that yielded the median S_0 value.

ACPD
11, 15875–15920, 2011

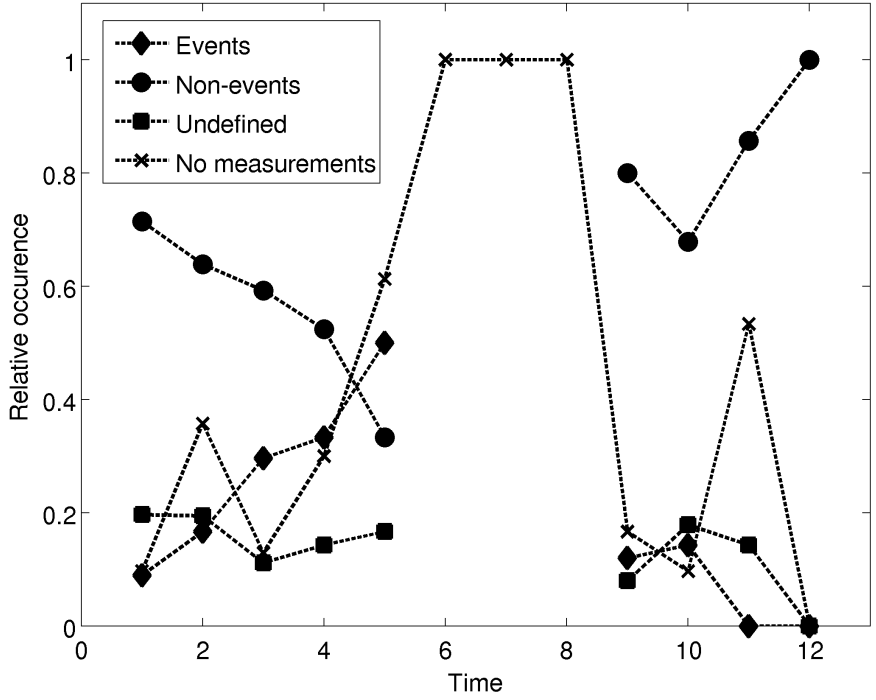

Fig. 4. Relative occurrence of event, non-event, undefined and without-measurements days as a function of the month of the year.

ACPD
11, 15875–15920, 2011

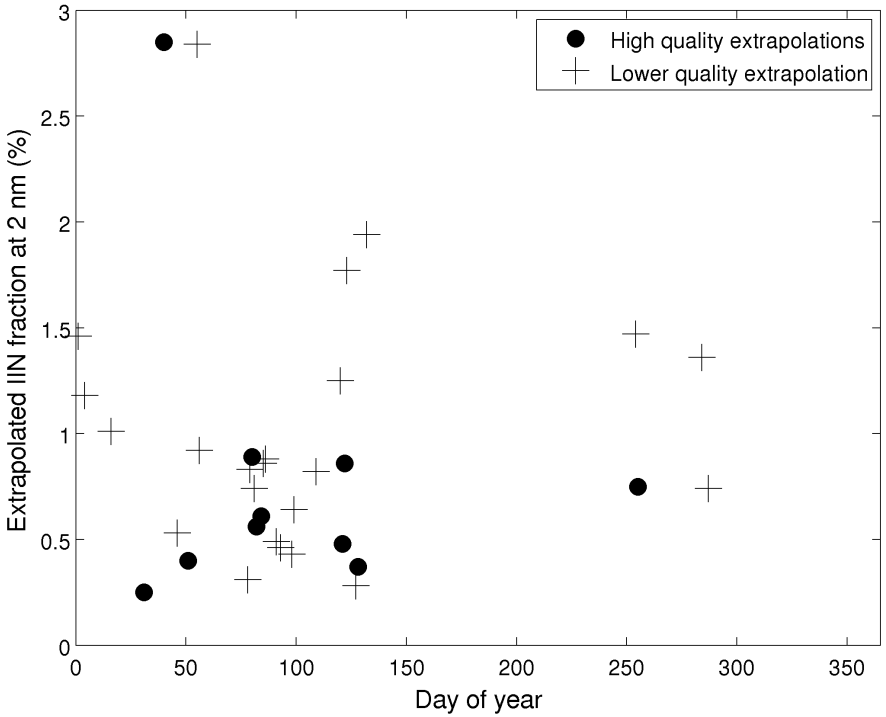

Fig. 5. Extrapolated ion-induced contribution at 2 nm as a function of the day of the year. The ion-induced contribution is calculated from the sum of the extrapolated negative and positive ion-induced fraction at 2 nm. High quality extrapolations are those from days on which both the negative and positive fit quality value were one. All other ion-induced fractions are in the lower quality extrapolation category.

ACPD
11, 15875–15920, 2011

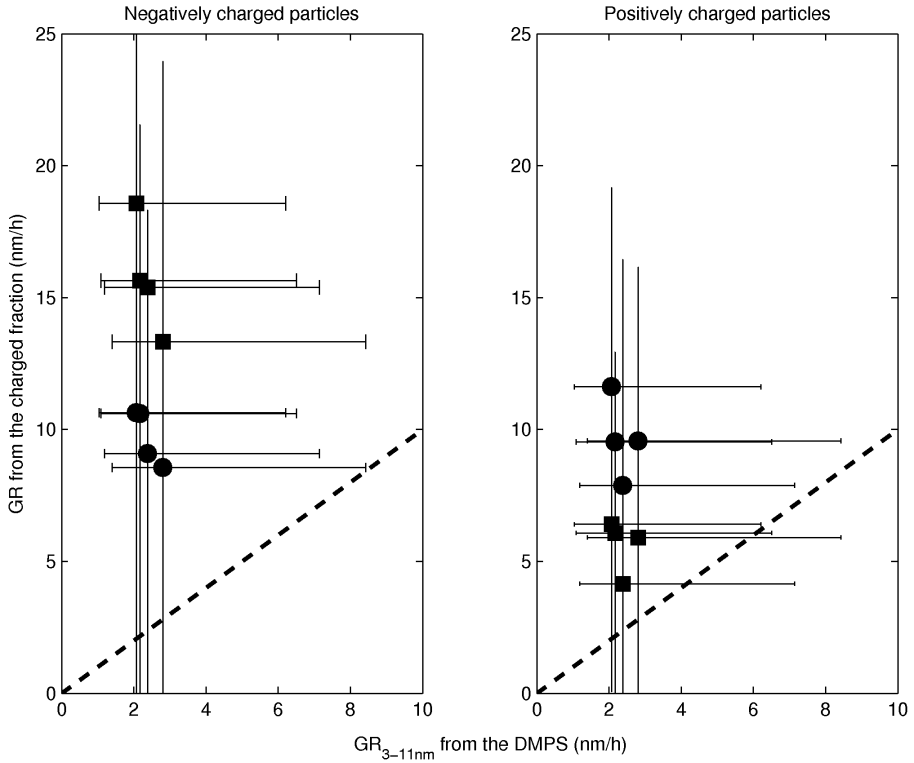

Fig. 6. Growth rate (GR_f) calculated from the charging ratios as a function of the growth rate (GR_{PSD}) between 3 and 11 nm for the five listed days that also belong to the DMPS class I. The circles represent the growth rates of the asymmetric case and the squares represent the symmetric case. The error bars for GR_{PSD} is a factor of two, and the error bars for GR_f are the 25th and 75th percentile of growth rates fitted through randomly generated points in the uncertainty boxes of the charged fraction as a function of the diameter.

ACPD
11, 15875–15920, 2011